Computer Simulations of the OmpF Porin from the Outer Membrane of *Escherichia coli*

Masakatsu Watanabe,* J. Rosenbusch,# T. Schirmer,# and Martin Karplus*§

*Department of Chemistry and Chemical Biology, Harvard University, Cambridge, Massachusetts 02138 USA; #Biozentrum, University of Basel, CH-4056 Basel, Switzerland; and §Laboratoire de Chimie Biophysique, Institut Le Bel, Université Louis Pasteur, 67000 Strasbourg, France

ABSTRACT Molecular dynamics simulations were used to study the structure and dynamics of the *Escherichia coli* OmpF porin, which is composed of three identical 16-stranded β-barrels. Simulations of the full trimer in the absence of water and the membrane led to significant contraction of the channel in the interior of each β-barrel. With very weak harmonic constraints (0.005 kcal/mol Å^2/atom) applied to the main-chain C_α atoms of the β-barrel, the structure was stabilized without alteration of the average fluctuations. The resulting distribution of the fluctuations (small for β-strands, large for loops and turns) is in good agreement with the x-ray B factors. Dynamic cross-correlation functions showed the importance of coupling between the loop motions and barrel flexibility. This was confirmed by the application of constraints corresponding to the observed temperature factors to the barrel C_α atoms. With these constraints, the β-barrel fluctuations were much smaller than the experimental values because of the intrinsic restrictions on the atomic motions, and the loop motions were reduced significantly. This result indicates that considerable care is required in introducing constraints to keep proteins close to the experimental structure during simulations, as has been done in several recent studies. Loop 3, which is thought to be important in gating the pore, undergoes a displacement that shifts it away from the x-ray structure. Analysis shows that this arises from the breakdown of a hydrogen bond network, which appears to result more from the absence of solvent than from the use of standard ionization states for the side chains of certain β-barrel residues.

INTRODUCTION

Porins are proteins that form channels across outer membranes of Gram-negative bacteria (Jap and Walian, 1990; Schirmer and Rosenbusch, 1991; Nikaido, 1993; Cowan, 1993). They act as sieves that allow polar molecules with masses of less than 600 Da to pass through the membrane. In this way, the porins mediate the import of nutrients and the export of waste products. Several porins from *Escherichia coli* share a high degree of sequence homology (Mizuno et al., 1983; Jeanteur et al., 1991) that is absent from an unrelated maltose-induced porin from *E. coli* (Clément and Hofnung, 1981), and from two porins from photosynthetic bacteria (Schiltz et al., 1991). Their tertiary structures nevertheless exhibit a similar architecture (Pauptit et al., 1991), a finding in accord with the high-resolution structures of OmpF-porin and phosphoporin (Cowan et al., 1992), of maltoporin (Schirmer et al., 1995) and of the porins from *R. capsulatus* and *Rsp. blastica.* (Weiss et al., 1991). Porins from *E. coli* exhibit cation and anion selectivity (OmpF-porin and phosphoporin, respectively) and are solute-specific in the case of maltoporin. Moreover, mutants may easily be constructed in *E. coli*, and selective pressure may be applied to assess the physiological significance of the alterations. Single-channel recordings show changes in channel function at the molecular level, and monitoring solute transport reveals modification of the exclusion limit and solute specificity.

Most porins have trimeric β-barrel structures, and the number of strands forming the barrels is variable. The β-barrel consists of 16 strands in OmpF-porin and phosphoporin, and 18 strands in maltoporin. Other proteins in the outer membrane have been predicted to contain 8–32 β-strands. The β-barrels have one loop that extends into the interior of the channels and constricts the narrow part to an opening of 7 × 10 Å^2 in Omp F porin. This is likely to contribute to the selectivity and size exclusion of the pore. Additional loops reduce the site of the constriction in other porins; e.g., in maltoporin, the size is reduced to 5 × 5 Å^2, with a corresponding reduction of the channel conductance by a factor of 5. Voltage gating has been found in several, although not all, porins (Schindler and Rosenbusch, 1978, 1981; Dargent et al., 1987; Mauro et al., 1988; Lakey and Pattus, 1989; Buehler et al., 1991). The constricting loops may be involved in the mechanism of voltage gating. The physiological significance of the voltage-dependent behavior is not known (Nikaido, 1993; Rosenbusch, 1994).

A detailed understanding of the mechanism of translocation in the cation- and anion-selective porins is not yet available. Theoretical studies of the mechanism at the atomic level by molecular dynamics simulation methods can complement the structural data. In this paper, which represents the first step in the simulation of porin dynamics, we focus on the OmpF porin from *E. coli*. It has three identical subunits, each of which is a 16-stranded β-barrel. There are eight loops of varying length at the (external) entrance, whereas there are only short turns on the periplas-

Received for publication 18 June 1996 and in final form 10 January 1997.

Address reprint requests to Dr. Martin Karplus, Department of Chemistry, Harvard University, 12 Oxford St., Cambridge, MA 02138. Tel.: 617-495-4018; Fax: 617-495-1792; E-mail: marci@tammy.harvard.edu.

0006-3495/97/05/2094/09 $2.00

mic side. X-ray crystallographic results reveal that the third loop (L3) folds into the channel (Cowan et al., 1992). Unlike the other loops, loop 2 (L2) bends away from the channel axis and extends into the neighboring subunit. A salt bridge of a glutamyl residue on L2 with cationic groups in the channel lumen of a neighboring subunit is the only electrostatic interaction between subunits; all other interactions are hydrophobic. The subunits pack tightly by interdigitation of side chains. This coexistence of hydrophobic and electrostatic interactions leads to a highly stable protein. Furthermore, it suggests that the monomer should be examined by molecular dynamics as part of the trimer.

The next section describes the model and methods used in the molecular dynamics simulations. The results obtained concerning the stability of the structure and the atomic fluctuations are presented in the third section. The dynamics of the loops and β-strands are compared with the x-ray data. Studies by Biörkstén et al. (1994) of the vacuum dynamics of the related porin from *R. capsulatus* are briefly discussed.

MODEL AND METHOD

The CHARMM program (Brooks et al., 1983) with the CHARMM19 parameter sets was used for all calculations Neria et al. 1996). A distance-dependent dielectric ($\epsilon = R$) was used. The OmpF model includes all heavy polar atoms and all polar hydrogens; aliphatic hydrogens are treated as parts of the carbon to which they are attached (extended atom model). The OmpF porin structure determined at 2.4 Å resolution by Cowan et al. (1992) is used as the starting point of the calculations (see Fig. 1). Each monomer consists of 340 amino acid residues, and there is a total of 9687 atoms in the trimer. The amino acid sequence is shown in Table 1, which also indicates the distribution of the amino acids among β-sheets, turns, and loops.

Polar hydrogen atoms were added to the porin crystal coordinates by use of the HBUILD facility in the CHARMM program. To remove local strains due to the addition of the hydrogen atoms, the resulting OmpF porin was minimized for 200 steps, with the Adapted Basis Newton Raphson (ABNR) algorithm (Brooks et al., 1983) keeping all heavy-atom positions fixed. All ionizable groups were given standard charges corresponding to pH 7; i.e., Glu, Asp, Lys, Arg, and the termini are ionized. Because of the presence of charge clusters involving several Arg and Lys and hydrogen-bonded networks involving Glu and Asp, the standard charge states may not be appropriate. Continuum electrostatic calculations by Karshikoff et al. (1994) suggest that some of the Glu, Asp, and Arg are neutral at pH 7, the pH at which most of the experiments are done. Thus most of the present simulations provide information on the effects of the standard charged states on the behavior of these clusters and their effect on the structure and dynamics of the system. Addtional simulations which examine alternative charge states are described briefly in the Discussion.

The IMAGE facility of the CHARMM program was used to generate the trimer by rotating the primary porin monomer (see Fig. 1) about the C_3 symmetry axis at the center of the molecule. To remove strain in the trimer generated in this way, a series of ABNR minimizations were applied to the system. They consisted of 150 steps with all heavy atoms fixed, 150 steps with all main-chain atoms fixed, and finally 150 steps with only the C^{α} atoms fixed. The final structure from the energy minimization was used as the

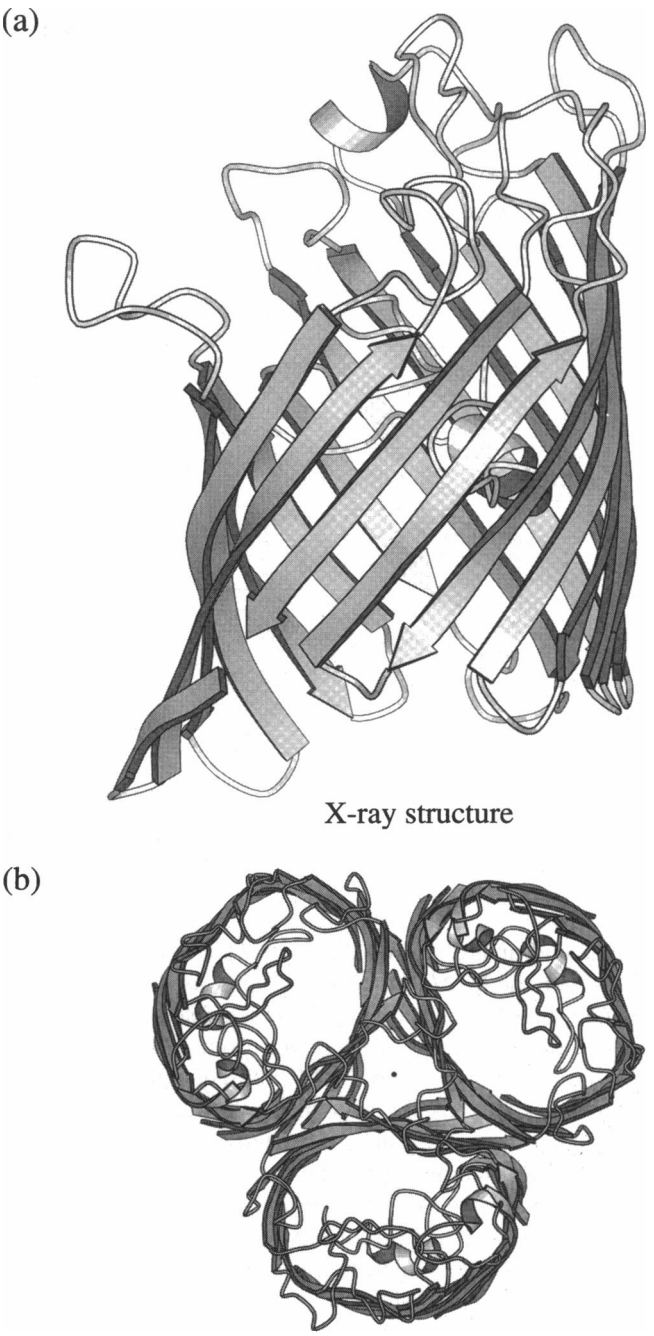

FIGURE 1 Ribbon diagrams of the OmpF porin corresponding to the x-ray structure. (*a*) View of a monomer from within the plane of the membrane toward the face of the barrel. (b) View of the trimer looking down the threefold axis, which is represented by a circle in the center of the trimer. These figures were drawn with the program MOLSCRIPT (Kraulis, 1991).

TABLE 1 Sequence and structure of porin monomer

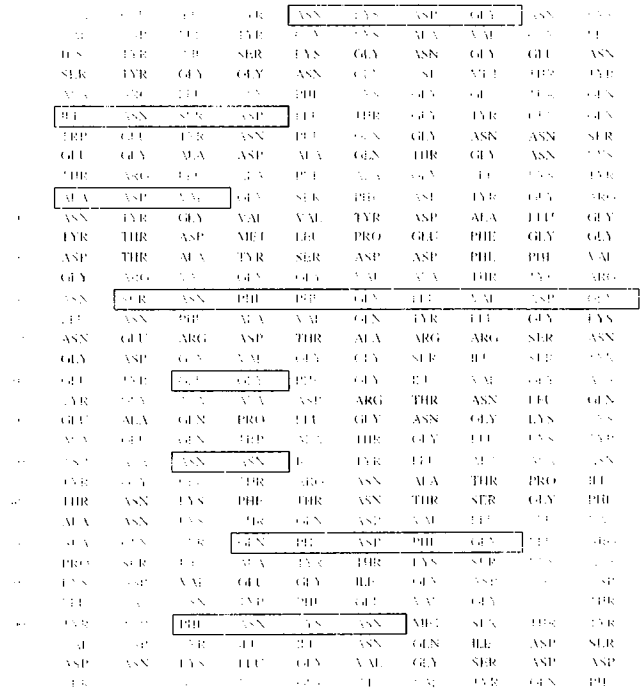

Gray shaded areas indicate the 8 loops in the entrance of the OmpF porin; the small turns at the periplasmic side of porin are indicated by the boxes; the other amino acids are associated with the 16 β-strands, except for the N and C termini.

initial coordinate set for the molecular dynamics simulations with the IMAGE module. In this way the full trimer is treated, but there are only 3229 independent atoms. Initial velocities were randomly assigned from a Gaussian distribution at a temperature of 300K. Subsequently, the temperature was kept constant by coupling the system to a thermal heat bath by use of the Nose-Hoover method (Hoover, 1985). The equations of the motions were integrated with a multiple time-step (MTS) algorithm (Watanabe et al., 1993, 1995) implemented in the CHARMM program (Brooks et al., 1983). In the algorithm, forces derived from bond-stretching and angle-bending motions are considered as hard forces and the rest of the forces as soft. Hard forces were integrated with a time step of 0.5 fs, and the soft forces were integrated with a time step of $\Delta t = 2$ fs. To account for significant contribution from long-range forces in this periodic system, a group-by-group-based cutoff of 12 Å was used for the Lennard-Jones and Coulomb interactions, with a smooth switching region of 4 Å obtained with the switching function in the CHARMM program (Brooks et al., 1983).

Several different simulations were carried out to investigate the stability of the system. Constraints on C^{α} atoms of the β-strands of the trimer were introduced to stabilize the pore. A harmonic potential was applied to the atoms; it has the form

$$U_i = K_i(r_i - r_i^{ref})^2, \quad (1)$$

where U_i is the potential energy applied to atom i, K_i is the force constant, and r_i and r_i^{ref} are the actual coordinates and the reference coordinates of atom i, respectively. In general, the effective force constant can be expressed by

$$K_i = \frac{k_B T}{2\langle \Delta \mathbf{r}_i^2 \rangle}, \quad (2a)$$

where Δr_i is a deviation from the reference position of atom i, and the brackets represent a time average. k_B is the Boltzmann constant, and T is the temperature. The value of $\langle \Delta r_i^2 \rangle$ can be estimated from the B factors via

$$\langle \Delta \mathbf{r}_i^2 \rangle = \frac{3B_i}{8\pi^2} \quad (2b)$$

(Brooks et al., 1989). The force constants used are given in Table 2.

RESULTS

Vacuum simulations without constraints

A 100-ps production run was performed with the MTS algorithm, and coordinates were saved every 0.1 ps for analysis. In the absence of constraints, the entire system can rotate about the threefold axis. To avoid complications in the analysis, any global rotation was removed every 500 steps of 2 fs by resetting the velocities of all atoms. The temperature of the system during the 100-ps simulation is plotted in Fig. 2 at 0.1-ps intervals. It shows that the Nose-Hoover thermostat preserves the temperature of the trimer in the vicinity of 300K; the temperature range is 300 ± 5K.

TABLE 2 Harmonic constraints and nature of simulations

Model	Force constant (kcal/mol Å^2)	Time step* (fs)	Total length (ps)	Description of constrained atoms
1	1.20	2.0 (0.5)	75	All mainchain atoms of β-sheets and turns
2	K_i#	2.0 (0.5)	100	C^{α} atoms on the outside part of β-barrel§
3	0.005	2.0 (0.5)	100	C^{α} atoms on the outside part of β-barrel§

*Integration of the equations of motions was performed by the MTS method (see text): numbers in parentheses correspond to the time steps for the hard forces (see text).

#The force constant of each assigned C^{α} atom is different, in accord with Eq. 2 (see text).

§Residues in the outside part of β-barrel are defined in the text.

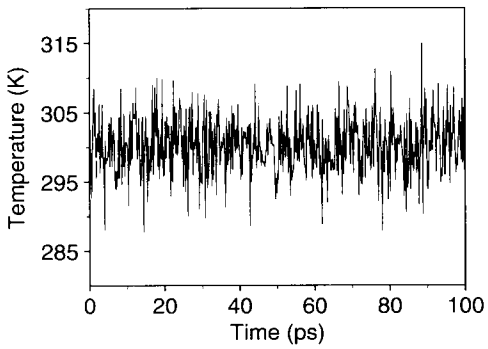

FIGURE 2 Temperature of the OmpF porin trimer in the unconstrained simulation as a function of the simulation time; the same stable behavior is observed in all of the simulations.

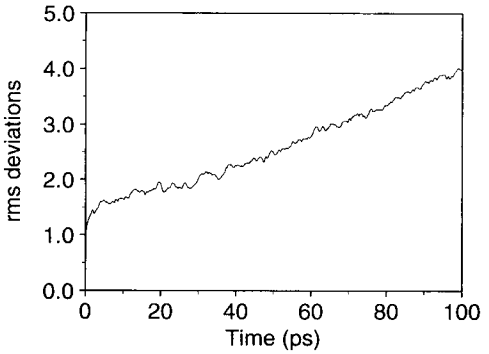

FIGURE 3 The averaged rms difference (Å) of the backbone atoms of the β-barrel from the x-ray structure in the unconstrained simulation as a function of the simulation time.

Table 3 presents the root mean square (rms) differences from the x-ray structure of average structures for different times; the values from the 40-ps equilibration period are included. When the x-ray structure is compared with the averaged coordinates obtained from the entire 100-ps simulation, the rms difference for all atoms is 3.1 Å. For the backbone atoms, the rms deviations for the β-barrel are considerably smaller than those in the loops or turns. However, the most important point is that the deviations of the backbone atoms of the β-barrel increase monotonically over the entire simulation (see Fig. 3). The deviation reaches 4.0 Å at 100 ps, and there are no indications that the structure is becoming stabilized during the trajectory.

The radius of gyration R_G of the experimental structure is equal to 20.7 Å for all atoms and to 19.0 Å for the main-chain atoms in the β-barrel. During the 40 ps of heating and equilibration, R_G changed from 20.4 to 19.9 Å for all atoms and from 18.8 Å to 18.5 Å for the main-chain atoms in the β-barrel. R_G continued to decrease for the first 60 ps of the production run. After that, it reached a relatively stable value of 19.6 Å for all atoms and 18.1 Å for the β-barrel main-chain atoms.

The contraction corresponding to the decrease in R_G is evident in the structure (Fig. 4 *a*). The outside region of the barrel (at the bottom of Fig. 4 *a*) is exposed to vacuum. Part of the reduction of the R_G value including all heavy atoms is due to the folding in of surface side chains. However, the largest shifts occurred on the outside of the β-barrel, whereas the region of the subunit interface was stable. Biörkstén et al. (1994) performed a vacuum simulation of a single porin of *R. capsulatus*, which has a topology similar to that of the OmpF porin. They observed much larger contractions of the β-barrel, but in preliminary results for the trimer, they obtained values for R_G that are similar to those in the present simulation. In the membrane, the β-barrel is stabilized by the presence of phospholipid molecules outside the trimer and by solvent inside the pore.

TABLE 3 Root mean square differences (in Å) between the x-ray structure and the 100-ps simulation without constraints*

Time period	All*	Side chain	Backbone β-Strands	Backbone Loops and turns
X-ray vs				
(0–100)	3.126	3.420	2.412	3.278
(0–25)	2.566	2.864	1.588	2.894
(25–50)	2.904	3.212	2.099	3.096
(50–75)	3.515	3.810	2.811	2.655
(75–100)	4.127	4.403	3.589	4.165
Initial#	2.131	2.430	0.867	2.556

*Averaged over all atoms, except hydrogen atoms.
#Initial corresponds to the end of the heating and equilibration period prior to the 100-ps simulation.

The mean square (MS) fluctuations of atoms in a protein can be estimated from the x-ray temperature factors (Brooks et al., 1989), as in Eq. 2b, although the temperature factors include disorder contributions as well as the actual internal fluctuations. The mean square fluctuations per residue, estimated from the x-ray atomic temperature factors averaged over the backbone atoms, are plotted in Fig. 5; the β-strand, loop, and turn regions are indicated in the figure. There is a striking difference between the β-strand values and those for loops and turns. The mean square fluctuations for the backbone atoms calculated from the 100-ps simulation are shown in Fig. 6 *a*. The simulation results are in accord with the variation along the chain found in the x-ray analysis. However, most of the calculated values are significantly larger than those found experimentally. Because the deviation of the simulation structure from the x-ray structure increases with time (Fig. 3), the calculated mean square fluctuations contain contributions from both the real atomic fluctuations about local minima and the changes that occur because of the structural drift. This is confirmed by the much smaller fluctuations obtained from two 50-ps subaverages. This reduction arises from the fact that the rms difference between the two average structures is 0.65 Å.

Simulations with harmonic constraints

To stabilize the porin trimer, we introduced terms to restrain the β-barrel main-chain atoms into the potential function. It

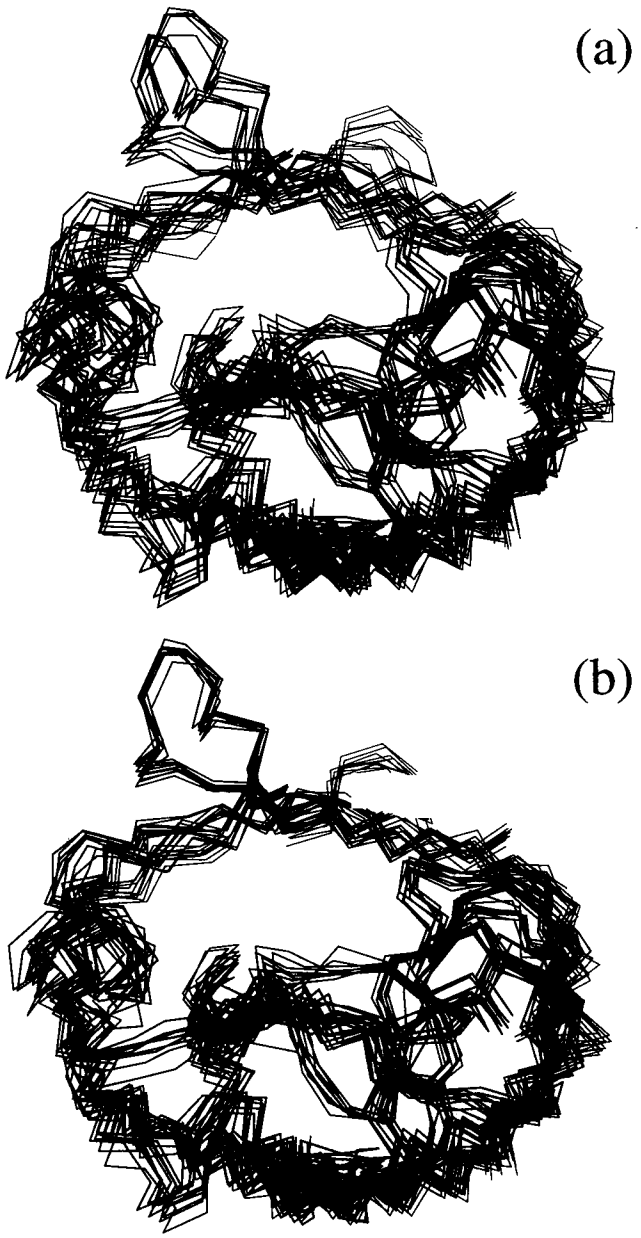

FIGURE 4 C_α backbone from the 100-ps simulations (10 traces at 10-ps intervals). (*a*) The unconstrained simulation; (*b*) the simulation with weak (0.005 kcal/mol-Å^2) constraints. The outside of the trimer is at the bottom in each case. These figures were drawn with the program MOLSCRIPT (Kraulis, 1991).

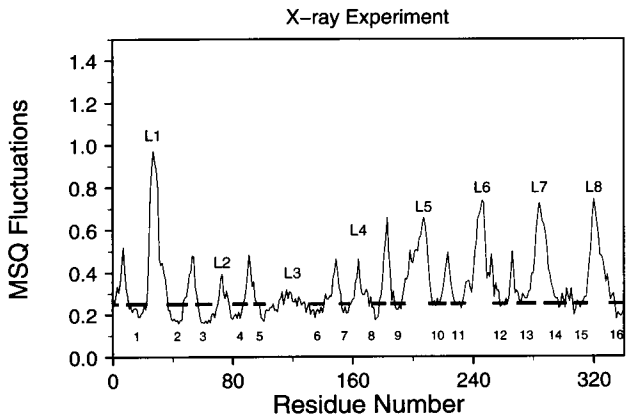

FIGURE 5 Mean square fluctuations (Å^2), $\langle(\Delta r)^2\rangle = \langle(\Delta R)^2\rangle/3$, obtained from x-ray temperature factors of the backbone atoms (C^α, C, O, and N) averaged on a per-residue basis for the OmpF porin. Dark thick lines at the bottom of the plot represent the positions of the 16 β-strands of the barrel; the symbols L1, L2, ... above some peaks indicate the positions of the 8 loops.

is known that the porin trimers in the membrane are very stable; e.g., the structure is not destroyed at rather high temperature (70°) and in the presence of detergents (Rosenbusch, 1974; Schindler and Rosenbusch, 1984). The restraints compensate for the absence of the exterior membrane and interior water. Similar restrained simulations have been used for the gramicidin channel in the absence of a membrane environment (Chiv et al., 1989).

Three different sets of constraints (see Eq. 1) were examined to find conditions that stabilize the porin trimer without significantly altering the intrinsic dynamics. The three models are listed in Table 2. The same integration scheme was used as for the free dynamics; the harmonic constraints are treated as hard forces in the MTS algorithm (see Model and Methods). In model 1, a single force constant obtained by averaging over the experimental temperature factors was applied to all main-chain atoms of the β-strands and the turns on the periplasmic side; no constraints were applied to the loops. In model 2, harmonic constraints with the force constants obtained from the individual temperature factors (see Eq. 2) were applied to the C^α atoms on the outside of the β-barrel, which had been shown to undergo the main distortions in the unconstrained simulation (Fig. 4 *a*). The outer portion of the β-barrel is defined as the region in contact with membrane lipids. It includes 10 of the β-strands (132–141, 151–158, 173–182, 185–195, 210–222, 225–235, 253–263, 269–283, 287–302, and 307–316) and excludes those involved in subunit contacts. A total of 125 C_α atoms were constrained. Finally, in model 3 a very small force constant (K = 0.005 kcal/mol-Å^2) was applied to the same C^α atoms as in model 2. This value corresponds to $\langle\Delta r^2\rangle$ for an isolated C^α harmonic oscillator equal to 59.6 Å^2 at 300K. Thus it is expected that it will not alter the intrinsic fluctuations, which from experiment are on the order of 0.815 Å^2 for the β-strand main-chain atoms; the calculated value is 1.01 Å^2.

Fig. 6 *b* shows the mean square fluctuations of the backbone atoms over a 75-ps simulation with model 1. It is clear that the β-barrel is too rigid, with atomic fluctuations that are much smaller than those corresponding to the temperature factors. The fluctuations of most of the loops are also significantly smaller than the values estimated from the temperature factors and obtained in the unconstrained simulation. Because the loops themselves were not constrained, this indicates that the fluctuations of the β-strands are important for the dynamics of the loops. Model 2, although less unrealistic than model 1, was still too rigid. The results

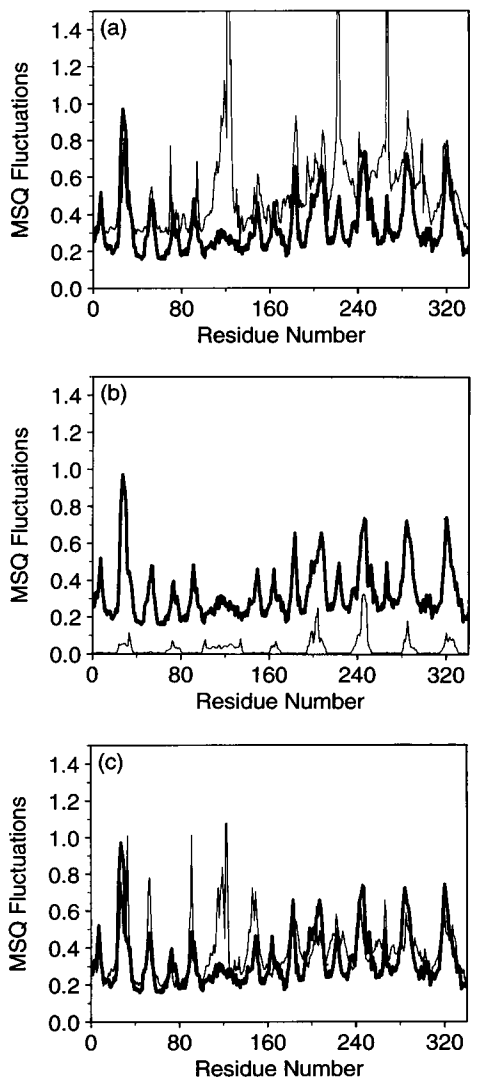

FIGURE 6 Mean square fluctuations of the backbone atoms averaged on a per-residue basis. (*a*) The unconstrained trimer simulation (*thin line*); (*b*) the constrained (model 1) trimer simulation (*thin line*); (*c*) the constrained (model 3) trimer simulation (*thin line*). The thick line corresponds to the x-ray values (see Fig. 5).

for both models 1 and 2 are in accord with the fact that the intrinsic motional constraints inherent in the structure add to the external constraints and significantly reduce the calculated motions, relative to those corresponding to the harmonic force constants.

Model 3 has constraints that are so small that they should affect the local fluctuations. Consequently, it is necessary to ascertain only that they are sufficient to preserve the structural integrity of the trimer. R_G values corresponding to the average structure generated during the 100 ps are plotted in Fig. 7. After 20 ps of production, the R_G value is stabilized at 19.7 Å, in satisfactory agreement with experiment. The root mean square deviations from the x-ray results of structures averaged over different portions of the 100-ps simulation are presented in Table 4; they are more stable than

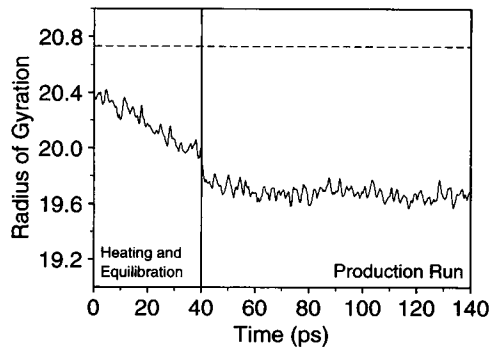

FIGURE 7 Radius of gyration (Å), for model 3 calculations of the OmpF porin as a function of the simulation time. These values are calculated by using all atoms in the OmpF porin.

those from the unconstrained dynamics (Table 2). Fig. 4 *b* shows the overlay of 10 structures from the 100-ps constrained simulation. In contrast to Fig. 4 *a* from the unconstrained simulation, there is somewhat less deformation.

Dynamics of the OmpF porin from model 3

The mean square fluctuations from the weakly constrained simulation are shown in Fig. 6 *c*. There is a clear difference between the small fluctuations of the β-strands of the barrel, as well as the turns, and the large fluctuations of the loops. In most cases there is good agreement with the x-ray temperature factors for the magnitude of fluctuations. For loop L3 the calculated fluctuations are significantly larger than those from the x-ray temperature factors. We discuss this result below.

The importance of collective motions in the OmpF porin has been probed by determining the correlation of the fluctuations of the different residues, calculated relative to the centers of mass (McCammon, 1984; Ichiye and Karplus, 1991). The dynamic cross-correlation between residues *i* and *j*, C_{ij}, is given by

$$C_{ij} = \frac{\langle \Delta r_i \cdot \Delta r_j \rangle}{\sqrt{\langle \Delta r_i^2 \rangle \langle \Delta r_j^2 \rangle}}, \qquad (3)$$

TABLE 4 Root mean square differences (in Å) between the x-ray structure and the 100-ps simulation with harmonic constrains (K = 0.005 kcal/mol)*

Compared time period	All	Side chain	Backbone	
			β-Strands	Loops and turns
X-ray vs				
(0–100)	2.630	2.945	1.448	3.064
(0–25)	2.524	2.807	1.347	3.006
(25–50)	2.701	3.031	1.541	3.099
(50–75)	2.721	3.059	1.531	3.124
(75–100)	2.779	3.111	1.537	3.237
Initial#	2.359	2.659	1.006	2.871

*Averaged over all atoms, except hydrogen atoms.
#Initial corresponds to the end of the heating and equilibration period before the 100-ps simulation.

where Δr_i is the instantaneous displacement of residue i from its average position. The values of C_{ij} can vary from 1 (perfect correlation) through 0 (no correlation) to -1 (perfect anticorrelation). A standard contact map for the residues based on the simulation is shown in Fig. 8 *a*, and the dynamic correlations are shown in Fig. 8 *b*. The contact map (Fig. 8 *a*) clearly shows several characteristics of the OmpF porin structure. The 16 β-strands appear as short dark lines perpendicular to the diagonal. The contacts between loop L3 (residues 103–131) and the strands of the β-barrel are visible. There are also a number of small off-diagonal contact elements. The elements near (25, 330) correspond to the interaction between the first and 16th β-strands. Loop L1 is interacting with the L6 and L8 at points (30, 24) and (30, 32), loop L4 with L6 near (1 65, 240), L5 with L6 near (200, 285), and L6 with L8 near (240, 320). Loop L2 is extended toward the neighboring porin, so that it has essentially no interactions with its own porin. These loop interactions are observed in the x-ray structure (Cowan et al., 1992).

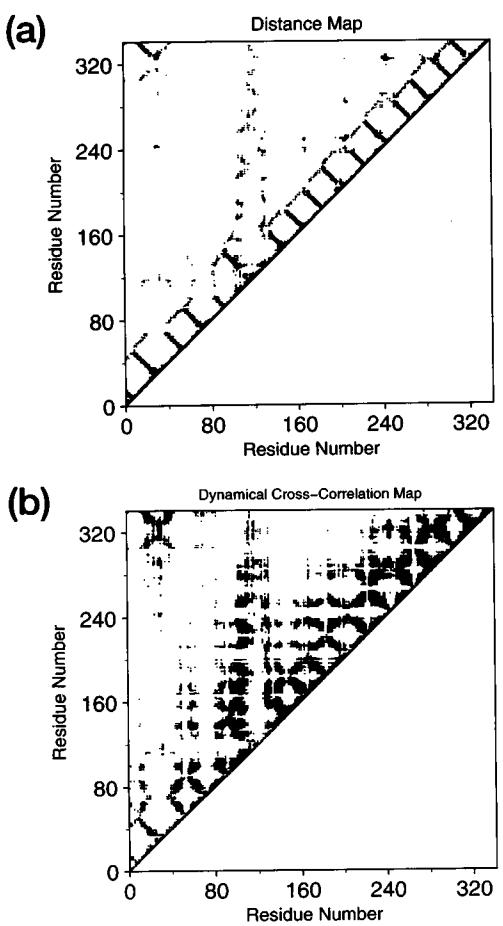

FIGURE 8 Residue interaction maps. (*a*) Distance map from 100-ps simulation average; distances less than 10 Å between the centers of mass of the residues are shown. (*b*) Dynamical cross-correlation map based on instantaneous displacements of the centers of mass from their average positions averaged over the 100-ps simulation (see Eq. 3); only elements that have values larger than 0.7 are shown.

The cross-correlation map (Fig. 8 *b*), when compared with Fig. 8 *a*, clearly shows that the correlations depend primarily on the distances. The dynamic cross-correlations are mainly positive; there are no significant negative correlations. Each β-strand correlates with the neighboring β-strands. The β-strands of the outside portion of the barrel have correlations beyond the neighboring strands; e.g., the 11th β-strand has strong dynamic correlations not only with the neighboring strands (10 and 12), but also with 9 and 13. The β-strands of the inside portion of the barrel wall have less correlation with the β-strands beyond the nearest neighbor. One reason for this is that the inside strands have strong correlations with the β-barrel of the other porins in the trimer. The only loop that has significant correlations with other parts of the porin is L3. This is in accord with the observation (see above) that the dynamics of loop L3 is strongly influenced by the barrel motions. Its dynamics is coupled to the motions of β-strands on the outside wall of the β-barrel, but there is very little correlation with the inside wall of the β-barrel (defined as β-strands 1 through 4); this is in accord with the position of loop L3.

DISCUSSION

As a first step in the analysis of porin dynamics, we have presented results from molecular dynamics simulations of the *E. coli* OmpF porin trimer in vacuum. An unconstrained 100-ps simulation shows considerable instability, presumably because of the absence of the interior waters and the exterior membrane environment. Very weak harmonic constraints applied to the C_α carbons in the outer β-barrel wall stabilized the system without significantly altering the local fluctuations. Overall, the structural and dynamic results of the simulation agree well with the x-ray data. Of particular interest is the reproduction of the small β-strand fluctuations and the much larger fluctuations in the connecting loops, which creates a striking pattern in the experimental and calculated results. If the β-barrel is rigidified by introducing larger harmonic constraints, the unconstrained loop fluctuations are significantly reduced, demonstrating a strong coupling between loop and barrel motions. When the experimental temperature factors are introduced as constraints, the calculated fluctuations are much smaller because of the intrinsic constraints on the motions. This implies that simulations which introduce x-ray (Romo et al., 1995) or NMR (Brunne et al., 1995) constraints to keep the structure near the experimental value must be evaluated with care to demonstrate that fluctuations are not overconstrained.

Loop L3 is in contact with the wall of the pore in the x-ray structure (Fig. 9 a). In the simulations this loop moves away from the wall and into the channel, so that the open space is smaller. This may represent the type of motion that occurs in the gating of the channel. Hydrogen bonds between the NH's of loop residues Glu 117, Phe 118, and the Asp 312 side chain of the barrel wall are broken during the simulation. These are replaced by hydrogen bonds between

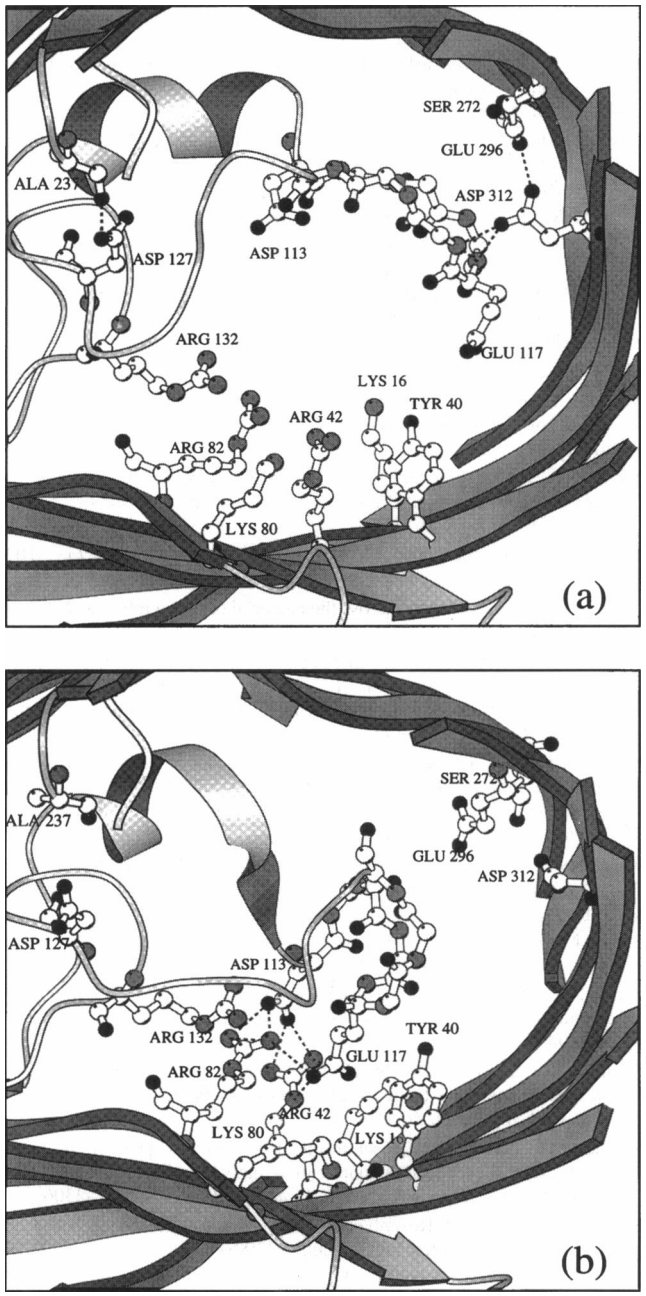

FIGURE 9 Diagram showing the β-barrel structure, with emphasis on loop L3 and key residues. (*a*) X-ray structure and (*b*) average structure from the last 10 ps of the trajectory (90–100 ps). These figures were drawn with the program MOLSCRIPT (Kraulis, 1991).

loop residues Asp 113 and Arg 132, as well as between Asp 132 and Arg 82, Arg 42 of the opposite channel wall (Fig. 9 *b*). Moreover, Glu 117 forms hydrogen bonds to Arg 42 and 82; in the x-ray structure Glu 117 appears to form hydrogen bonds with other porin residues (Tyr 22, Tyr 310). Simultaneously, the networks involving Ser 272, Glu 296, and Asp 312 on the outside of the barrel and Arg 42, Arg 82, Lys 16, and Lys 80 on the inside of the barrel are disrupted.

The observed behavior of loop L3 and the hydrogen bond networks is not unexpected. Karshikoff and co-workers (Karshikoff et al., 1994) have applied a continuum electrostatic model to the OmpF porin and suggested that either Glu 296 or Asp 312 or both are protonated because the carboxyl groups are at a distance corresponding to a hydrogen bond. They suggested a possible scheme for a hydrogen bond network involving loop L3 (see Fig. 3 of their paper and Fig. 9 *a*). In the present simulations all of the acidic groups were assumed to be in their standard ionization states and the hydrogen bonding networks were disrupted. The structures at 50 ps (not shown) and 100 ps (Fig. 9 *b*) show that the hydrogen bond network is broken. The unprotonated residues of Asp 312 and Glu 296 move away from each other during the simulation, and Asp 312 approaches Ser 272. These residues occasionally make a hydrogen bond during the simulation (see Fig. 9 *b*). At the same time, loop L3 moves away from Asp 312 and makes new interactions with other residues. This provides more space between the internal loop portion of L3 and the barrel wall, and is a reason for the large mean square fluctations of L3 displayed in Fig. 6 *c*. The aromatic ring of Phe 118 shows a large wagging motion during the simulations.

Several mutants that alter one of the charged residues that have electrostatic interaction with loop L3 have been studied by Benson et al. (1988); they include Arg 42, 82, and 132 and Asp 113, each of which was replaced by an uncharged residue. These resulted in an increase in the pore size, based on structural and functional data (Cowan et al., 1992; Benson et al., 1988; Misra and Benson, 1988). The deletion mutants in loop L3, studied by Lon et al. (manuscript in preparation), produced a widening of the channel but did not alter the β-barrel structure or mobility.

Additional 100-ps simulations (manuscripts in preparation) of porin with alternative ionization states of certain residues have been completed in vacuum and with 36 crystal water molecules. In accord with the work of Karshikoff and the crystal structure, Asp 121, Asp 127, Asp 256, Glu 296, and Asp 312 were neutralized; i.e., they were treated as the acid with a proton on the appropriate oxygen. In the vacuum system, there was initially a hydrogen bond network between the loop L3 residues and the outer β-barrel wall corresponding to that suggested by the x-ray analysis. However, loop L3 still underwent a large displacement in the 100-ps simulation that shifted it away from the x-ray structure to narrow the channel significantly. The loop motion with the neutralized residues in vacuum was similar to that described for the system with the charged side chains. This indicates that the hydrogen bond network based on neutralized side chains is not sufficient, per se, to stabilize loop L3 in the open position. Additional simulations were carried out with the vacuum system plus 36 crystal waters; these water molecules are inside the β-barrel and many of them are in contact with loop L3. Both the unprotonated porin (i.e., with the acidic residues charged) and the protonated porin (with the acidic residues neutralized) were simulated for 100 ps. For both systems, loop L3 had no large displacements. In particular, Glu 117 and Phe 118, which are located a tip of loop L3, continued to make good

hydrogen bonds with Asp 312 of the β-barrel wall. Thus, in the presence of the crystal water molecules, there is no significant narrowing of the channel.

The results presented here will be supplemented by longer simulations of fully solvated porins with alternative ionization states for critical residues (work in progress).

The paper was supported in part by a grant from the National Science Foundation to MK and grants from the Swiss National Science Foundation to TS and JR.

REFERENCES

Benson, S. A., J. L. L. Occi, and B. A. Sampson. 1988. Mutations that alter the pore function of the OmpF porin of *Escherichia coli* K12. *J. Mol. Biol.* 103:961–970.

Biörkstén, J., C. M. Soares, O. Nilsson, and O. Tapia. 1994. On the stability and plastic properties of the interior L3 loop in *R. capsulatus* porin. A molecular dynamics study. *Protein Eng.* 7:487–493.

Brooks, B. R., R. E. Bruccoleri, B. D. Olafson, D. J. States, S. Swaminathan, and M. Karplus. 1983. CHARMM: a program for macromolecular energy, minimization, and dynamics calculations. *J. Comp. Chem.* 4:187–217.

Brooks, C. L., III, and M. Karplus. 1989. Solvent effects on protein motion and protein effects on solvent motion: dynamics of the active site region of lysozyme. *J. Mol. Biol.* 208:159–181.

Brooks, C. L., III, M. Karplus, and B. M. Pettitt. 1998. Proteins: a theoretical perspective of dynamics, structure, and thermodynamics. *Adv. Chem. Phys.* 72:1–259.

Brunne, B. M., K. D. Berndt, P. Güntert, K. Wüthrich, and W. F. van Gunsteren. 1995. Structure and internal dynamics of the bovine pancreatic trypsin inhibitor in aqueous solution from long-time molecular dynamics simulations. *Proteins Struct. Funct. Genet.* 23:49–62.

Buehler, L. K., S. Kusumotio, H. Zhang, and J. P. Rosenbusch. 1991. Plasticity of *Escherichia coli* porin channels: dependence of their conductance on strain and lipid environment. *J. Biol. Chem.* 266: 24446–24450.

Chiu, S. W., S. Subramanian, E. Jakobsson, and J. A. McCammon. 1989. Water and polypeptide conformations in the gramicidin channel. *Biophys. J.* 56:253–261.

Clément, J. M., and M. Hofnung. 1981. Gene sequence of the λ receptor, an outer membrane protein of *E. coli* K12. *Cell.* 27:507–514.

Cowan, S. W. 1993. Bacterial porins: lessons from three high-resolution structures. *Curr. Opin. Struct. Biol.* 3:501–507.

Cowan, S. W., T. Schirmer, G. Rummel, M. Steiert, R, Ghosh, R. A. Pauptit, J. N. Jansonius, and J. P. Rosenbusch. 1992. Crystal Structures explain functional properties of two *E. coli* porins. *Nature.* 358:727–733.

Dargent, B., J. P. Rosenbusch, and F. Pattus. 1987. Selectivity for maltose and maltodextrin of maltoporin, a pore-forming protein from *E. coli* outer membranes. *FEBS Lett.* 220:136–142.

Hoover, W. G. 1985. Canonical dynamics: equilibrium phase-space distributions. *Phys. Rev. A.* 31:1695–1697.

Ichiye, T., and M. Karplus. 1991. Collective motions in proteins: a covariance analysis of atomic fluctuations in molecular dynamics and normal mode simulations. *Proteins Struct. Funct. Genet.* 11:205–217.

Jap, B. K., and P. J. Walian. 1990. Biophysics of the structure and function of porins. *Q. Rev. Biophys.* 23:367–403.

Jeanteur, D., J. H. Lakey, and F. Pattus. 1991. The bacterial porin superfamily: sequence alignment and structure prediction. *Mol. Microbiol.* 51:2153–2164.

Karplus, M. 1981. Aspects of protein dynamics. *Ann. N.Y. Acad. Sci.* 367:407–418.

Karshioff, A., V. Spassov, S. W. Cowan, R. Ladenstein, and T. Schirmer. 1994. Electrostatic properties of two porin channels from *Escherichia coli. J. Mol. Biol.* 240:372–384.

Kraulis, P. J. 1991. MOLSCRIPT: a program to produce both detailed and schematic plots of protein structures. *J. Appl. Crystallogr.* 24:946–950.

Komeiji, Y., M. Uebayashi, and I. Yamato. 1994. Molecular dynamics simulations of *trp* apo- and holorepressors: domain structure and ligand-protein interaction. *Proteins Struct. Funct. Genet.* 20:248–258.

Lakey, J. H., and F. Pattus. 1989. The voltage-dependent activity of *Escherichia coli* porins in different planar bilayer reconstructions. *Eur. J. Biochem.* 186:303–309.

Levy, R. M., R. P. Sheridan, J. W. Keepers, G. S. Dubey, S. Swaminathan, and M. Karplus. 1985. Molecular dynamics of myoglobin at 298°K: results from a 300 ps computer simulation. *Biophys. J.* 48:509–518.

Mauro, A., M. Blake, and P. Labarca. 1988. Voltage gating of conductance in lipid bilayer induced by porin from outer membranes of *Neisseria gonorrhoeae. Proc. Natl. Acad. Sci. USA.* 85:1071–1075.

McCammon, J. A. 1984. Protein dynamics. *Rep. Prog. Phys.* 47:1–46.

Misra, R., and S. A. Benson. 1988. Genetic Identification of the pore domain of the OmpC porin of *Escherichia coli. J. Bacteriol.* 170: 3611–3617.

Mizuno, T., M.-Y. Chou, and M. Inouye. 1983. A comparative study on the genes for three porins of the *Escherichia coli* outer membrane. *J. Biol. Chem.* 258:6932–6940.

Neria, E., S. Fischer, and M. Karplus. 1996. *J. Chem. Phys.* 105: 1902–1921.

Nikaido, H. 1993. Transport across the bacterial outer membrane. *J. Bioenerg. Biomembr.* 25:581–589.

Pauptit, R. A., T. Schirmer, J. Jansonius, J. P. Rosenbusch, M. W. Parker, A. D. Tucker, D. Tsernoglou, M. S. Weiss, and G. E. Schulz. 1991. A common channel-forming motif in evolutionarily distant porins. *J. Struct. Biol.* 107:136–145.

Romo, T. D., J. B. Clarage, D. C. Sorensen, and G. N. Philipps, Jr. 1995. Automatic identification of discrete substates in porins: singular value decomposition analysis of time-averaged crystallographic refinements. *Proteins Struct. Funct. Genet.* 22:311–321.

Rosenbusch, J. P. 1974. Characterization of the major envelope protein from *Escherichia coli. J. Biol. Chem.* 249:8019–8029.

Rosenbusch, J. P. 1994. Porins. *In* Phosphate in Microorganisms. Celluar and Molecular Biology. A. Torriani-Gorini, E. Yagil and S. Silver, editors. ASM Press, Washington, DC. 329–334.

Schiltz, E., A. Kreusch, U. Nestel, and G. E. Schultz. 1991. Primary structure of porin from *Rhodobacter capsulatus. Eur. J. Biochem.* 199: 587–594.

Schindler, H., and J. P. Rosenbusch. 1978. Matrix protein from *Escherichia coli* outer membranes from voltage-controlled channels in lipid bilayers. *Proc. Natl. Acad. Sci. USA.* 75:3751–3755.

Schindler, H., and J. P. Rosenbusch. 1981. Matrix protein in planar membranes: clusters of channels in a native environment and their functional reassemble. *Proc. Natl. Acad. Sci. USA.* 78:2302–2306.

Schindler, H., and J. P. Rosenbusch. 1984. Structural transitions of porin, a transmembrane protein. *FEBS Lett.* 173:85–89.

Schirmer, T., T. A. Keller, Y. -F. Wang, and J. P. Rosenbusch. 1995. Structural basis for sugar translocation through maltoporin channels at 3.1 Å resolution. *Science.* 267:512–514.

Schirmer, T., and J. P. Rosenbusch. 1991. Prokaryotic and eukaryotic porins. *Curr. Opin. Struct. Biol.* 1:539–545.

Swaminathan, S., T. Ichiye, W. F. van Gunsteren, and M. Karplus. 1982. Time dependence of atomic fluctuations in proteins: analysis of local and collective motions in bovine pancreatic trypsin inhibitor. *Biochemistry.* 21:5230–5241.

Watanabe, M., and M. Karplus. 1993. Dynamics of molecules with internal degrees of freedom by multiple time-step methods. *J. Chem. Phys.* 99:8063–8074.

Watanabe, M., and M. Karplus. 1995. Simulations of macromolecules by multiple time-step methods. *J. Phys. Chem.* 99:5680–5697.

Weiss, M. S., U. Abele, J. Weckesser, W. Welte, E. Schiltz, and G. E. Schulz. 1991. Molecular architecture and electrostatic properties of a bacterial porin. *Science.* 254:1627–1630.